Solitons and four-wave mixing

Jay R. Ackerhalt
Los Alamos National Laboratory (Box 1663, Mail Stop J569), University of California, Los Alamos, New Mexico 87545

Peter W. Milonni*
Department of Physics, University of Arkansas, Fayetteville, Arkansas 72701
(Received 20 August 1985)

We develop the formalism for studying transient four-wave-mixing phenomena in a Raman medium, and apply it to the study of solitary-wave propagation. We consider the problems of second-Stokes generation, anti-Stokes scattering, and two-pump Raman scattering.

I. INTRODUCTION

Over the past few years the field of Raman solitons has received much attention following the observation of these solitons in a nondispersive medium by Carlsten, Wenzel, and Drühl in 1983.[1] Raman solitons were first discussed by Chu and Scott, Tan-no *et al.*, and Makhviladze *et al.* in 1975 and more recently by Kaup, Steudel, and Meinel.[2–4] Other work on Raman solitons has been done by Makhviladze and Sarychev,[5] who looked at soliton stability and dispersive effects, and by Hasegawa,[6] who considered propagation in optical fibers where dispersive effects are very strong.

Historically, these solitons were first observed to appear at random, roughly every twentieth shot, during Raman scattering experiments performed by Wenzel and Carlsten at Los Alamos.[7] In discussing this phenomenon with Drühl they learned about the work of Chu and Scott,[2] which showed that the pump was a hyperbolic secant function and the first-Stokes a hyperbolic tangent function. Since the hyperbolic tangent function is reminiscent of a function which simply changes sign or undergoes a π phase flip, Drühl in his computer model simply inserted this phase flip in the electric field envelope of the first-Stokes seed. The output of computer simulations showed that a soliton could be generated and located temporally so as to reproduce the experimental results. The next question asked was "Why did the soliton appear in the experiments at all?," since no effort was made to induce the soliton's formation. While the answer to this question is still under speculation, these solitons are now consistently generated experimentally by introducing a π phase shift in the first-Stokes seed pulse's temporal profile using a Pockels cell. Now that a reliable technique for generating these Raman solitons exists, new studies of the subtle details of soliton formation are being made both theoretically and experimentally.[8]

In this paper we will generalize the theoretical work on Raman solitons to include all four-wave-mixing phenomena which occur in a Raman medium. We plan to study three-field processes, i.e., second-Stokes generation and anti-Stokes scattering, and four-field processes, i.e., two-pump conversion. In Sec. II the equations of motion will be derived. In Sec. III we will discuss the essential physics of the four-wave-mixing process and the analytic calculation of mathematical soliton solutions. In Sec. IV computer generated simulations of these soliton processes will be shown. A summary will be presented in Sec. V.

There is one caveat to this work which must be understood before reading the paper. We are interested in the essential physics of four-wave-mixing processes in a Raman medium and soliton formation. Because of this goal we will not pursue fine details of the physical processes involved which are or may be relevant to the real world, but do not affect the fundamental physics of the process. Some examples of these details are complex field envelopes, gain parameters, field frequencies, bandwidths, field intensities, transverse beam profiles, dispersion, off-resonant detuning, etc.

II. EQUATIONS OF MOTION

A. Material medium

The essential physics of a Raman medium requires the existence of at least three energy states (0,1,2) where the highest-energy state (1) is electric-dipole coupled to the remaining two states (0,2). Only the ground state (0) is initially populated. For simplicity, we will assume the two transition dipole moments are equal ($\mu_{01}=\mu_{12}$) and equal to μ. The energy of state (1) (in frequency units) is ω_{01}. The energy of state (2) is Δ, and state (0), zero. In Fig. 1 we show this three-state system.

Since all the electric fields in the four-wave-mixing problems under consideration, i.e., pump, first-Stokes, second-Stokes, ..., first-anti-Stokes, etc., are potentially capable of coupling states (0-1) and (1-2), we will represent all of them generically by a single electric field $\mathbf{E}(z,t)$, where we are considering plane-wave propagation in the $\hat{\mathbf{z}}$ direction. Using the notation that n refers to a specific field, i.e., first-anti-Stokes, pump, first-Stokes, etc., we can define

$$\mathbf{E}(z,t)\equiv\tfrac{1}{2}\sum_n [\mathscr{E}_n(z,t)e^{i(k_n z-\omega_n t)} + \mathscr{E}_n^*(z,t)e^{-i(k_n z-\omega_n t)}] . \tag{2.1}$$

The quantities $\mathscr{E}_n$, k_n, and ω_n are the electric field en-

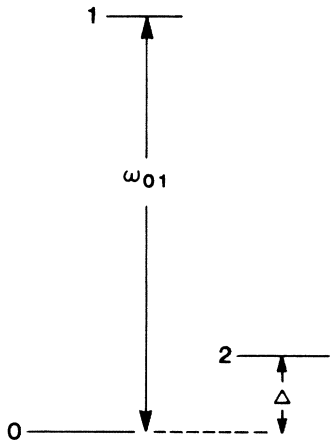

FIG. 1. Three-level system describing Raman medium.

velope, the wave vector, and frequency of the nth field. The electric fields are all linearly polarized in the same direction. Since we are not interested in generating the fields initially from noise, i.e., only from a seed pulse or four-wave mixing, we use classical fields.

The Hamiltonian for the material medium dipole coupled to the total electric field is

$$H=\omega_{01}|1\rangle\langle 1|+\Delta|2\rangle\langle 2| - \frac{\boldsymbol{\mu}\cdot\mathbf{E}(z,t)}{\hbar}(|1\rangle\langle 0|+|0\rangle\langle 1|+|1\rangle\langle 2| + |2\rangle\langle 1|) . \tag{2.2}$$

Specifying μ and $\mathbf{E}$ to be parallel allows us henceforth to drop the vector notation. The density-matrix equations generated from (2.2) using the notation

$$\rho_{ij}=\langle\psi|i\rangle\langle j|\psi\rangle \tag{2.3}$$

are

$$i\dot{\rho}_{11}=-\frac{\mu E(z,t)}{\hbar}(\rho_{10}-\rho_{01}+\rho_{12}-\rho_{21}) , \tag{2.4a}$$

$$i\dot{\rho}_{22}=\frac{\mu E(z,t)}{\hbar}(\rho_{12}-\rho_{21}) , \tag{2.4b}$$

$$i\dot{\rho}_{00}=\frac{\mu E(z,t)}{\hbar}(\rho_{10}-\rho_{01}) , \tag{2.4c}$$

$$i\dot{\rho}_{01}=\omega_{01}\rho_{01}+\frac{\mu E(z,t)}{\hbar}(\rho_{11}-\rho_{00}-\rho_{02}) , \tag{2.4d}$$

$$i\dot{\rho}_{12}=-(\omega_{01}-\Delta)\rho_{12} + \frac{\mu E(z,t)}{\hbar}(\rho_{22}-\rho_{11}+\rho_{02}) , \tag{2.4e}$$

$$i\dot{\rho}_{02}=\Delta\rho_{02}+\frac{\mu E(z,t)}{\hbar}(\rho_{12}-\rho_{01}) . \tag{2.4f}$$

Equations (2.4a)—(2.4c) conserve probability, $\rho_{00}+\rho_{11}+\rho_{22}=1$, making one of the equations redundant.

Since we are interested in studying off-resonant Raman scattering where the intermediate state (1) is never populated, we can adiabatically eliminate all of the variables which involve state (1) by assuming ω_{01} much greater than all other frequencies in the problem. Therefore, to lowest order in Δ/ω_{01} we find

$$\rho_{11}\cong 0 , \tag{2.5a}$$

$$\rho_{01}\cong\frac{\mu E(z,t)}{\hbar\omega_{01}}(\rho_{00}+\rho_{02}) , \tag{2.5b}$$

$$\rho_{12}\cong\frac{\mu E(z,t)}{\hbar\omega_{01}}(\rho_{22}+\rho_{02}) , \tag{2.5c}$$

where by working to this order of approximation we have neglected any possibility of Stark shifts in the final equations.

Substituting (2.5) into (2.4) we obtain a self-consistent set of equations describing the reduced two-level system (0,2):

$$\dot{Q}=-i(\Delta-\delta)Q-\Omega(z,t)e^{i\delta t}w , \tag{2.6a}$$

$$\dot{w}=2[\Omega(z,t)e^{-i\delta t}Q+\Omega(z,t)e^{i\delta t}Q^*] , \tag{2.6b}$$

where conservation of probability implies $\rho_{00}+\rho_{22}=1$. We have used the definitions

$$Q\equiv -ie^{i\delta t}\rho_{02} , \tag{2.7a}$$

$$w\equiv\rho_{22}-\rho_{00} , \tag{2.7b}$$

$$\Omega(z,t)\equiv\frac{1}{\omega_{01}}\left[\frac{\mu E(z,t)}{\hbar}\right]^2 , \tag{2.7c}$$

$$\delta\equiv\omega_n-\omega_{n+1}>0 , \tag{2.7d}$$

where n, as in (2.1), defines a specific field such that $n+1$ refers to its companion field with lower frequency, for example, if n defines the pump field, then $n+1$ defines the first-Stokes field. The frequency difference, $\Delta-\delta$, which is assumed small, is the frequency mismatch δ of nearest-neighbor field pairs, n and $n+1$, from the material medium's resonance at Δ. We have required that all the field pairs have the same detuning δ in order to simplify the problem. However, since we are always injecting a pump and first-Stokes field initially into the material medium with a well-defined detuning δ, we know that all subsequent four-wave-mixing processes will have their highest gain at the same detuning δ, substantiating this approximation.

The last step in reducing (2.6) is to select the time-independent rotating-wave-approximation (RWA) terms from the quantity $\Omega(z,t)e^{\pm i\delta t}$. All the other variables are already implicitly slowly varying. Using the definition of $E(z,t)$, (2.1), we obtain

$$\dot{Q}=-i(\Delta-\delta)Q-\frac{\mu^2}{2\hbar^2\omega_{01}}\left[\sum_{N,n}\mathscr{E}_{Nn}\mathscr{E}^*_{N,n+1}e^{i\Delta k_{Nn}z}\right]w , \tag{2.8a}$$

$$\dot{w}=\frac{\mu^2}{\hbar^2\omega_{01}}\left[Q^*\left[\sum_{N,n}\mathscr{E}_{Nn}\mathscr{E}^*_{N,n+1}e^{i\Delta k_{Nn}z}\right]+\text{c.c.}\right] . \tag{2.8b}$$

The indexing has been generalized such that the index N now refers to the Nth field chain defined by the Nth input pump field. This index is only required when there is more than one input pump field. The index n refers to the particular field in the Nth chain. The summation ($\sum_{N,n}$) is over all field pairs which match the two-photon transition. The quantity Δk_{Nn} is defined to be the differ-

ence in the field pair's wave vectors, $\Delta k_{Nn} \equiv k_{Nn} - k_{N,n+1}$. The quantity which appears in large parentheses in (2.8a) and (2.8b) represents the generalized complex Rabi frequency for this effective two-level system.[9] In order to simplify writing the equations we have dropped the explicit z and t dependence of $\mathscr{E}_{Nn}$.

There is one important effect missing from (2.8) which plays a major role in the experiments. It is the effect of collisions in the gas medium. To include this effect we simply introduce a dephasing rate constant $1/T$ into (2.8a) for the polarization. It is also possible to introduce population redistribution effects into (2.8), but these are not of any consequence here and, therefore, are not considered. The medium equations now become

$$\dot{Q} = -\left[i(\Delta-\delta)+\frac{1}{T}\right]Q - \frac{\mu^2}{2\hbar^2\omega_{01}}\left[\sum_{N,n}\mathscr{E}_{Nn}\mathscr{E}^*_{N,n+1}e^{i\Delta k_{Nn}z}\right]w \,, \tag{2.9a}$$

$$\dot{w} = \frac{\mu^2}{\hbar^2\omega_{01}}\left[Q^*\left[\sum_{N,n}\mathscr{E}_{Nn}\mathscr{E}^*_{N,n+1}e^{i\Delta k_{Nn}z}\right]+\text{c.c.}\right] . \tag{2.9b}$$

B. Maxwell's equations

In this part, since our fields are classical, we begin by using the second-order Maxwell equation for the electric field:

$$\left[\frac{\partial^2}{\partial z^2}-\frac{1}{c^2}\frac{\partial^2}{\partial t^2}\right]E(z,t) = \frac{4\pi}{c^2}\frac{\partial^2}{\partial t^2}P(z,t) \,, \tag{2.10}$$

where the polarization is obtained from (2.2),

$$P(z,t) = M\mu(\rho_{01}+\rho_{10}+\rho_{12}+\rho_{21}) \,, \tag{2.11}$$

M is the molecular density. Using relations (2.5b), (2.5c), and (2.7a) we obtain

$$P(z,t) = \chi E(z,t)(1+\rho_{02}+\rho_{20})$$

$$= \chi E(z,t) + i\chi[QE(z,t)e^{-i\delta t} - \text{c.c.}] \,, \tag{2.12}$$

where χ is the linear susceptibility of the medium ($\chi = 2M\mu^2/\hbar\omega_{01}$). Substituting (2.12) into (2.10) and using (2.1) we equate coefficients of all terms proportional to $e^{-i\omega_{Nn}t}$:

$$\left[\frac{\partial^2}{\partial z^2}-\frac{1}{c^2}\frac{\partial^2}{\partial t^2}\right][\mathscr{E}_{Nn}(z,t)e^{i(k_{Nn}z-\omega_{Nn}t)}]$$

$$= +\frac{4\pi}{c^2}\frac{\partial^2}{\partial t^2}\{\chi\mathscr{E}_{Nn}(z,t)e^{i(k_{Nn}z-\omega_{Nn}t)} + i\chi[Q\mathscr{E}_{N,n+1}(z,t)e^{i(k_{N,n+1}z-\omega_{Nn}t)} - Q^*\mathscr{E}_{N,n-1}(z,t)e^{i(k_{N,n-1}z-\omega_{Nn}t)}]\} \,. \tag{2.13}$$

By moving all terms not proportional to Q and Q^* from the right side to the left side of (2.13), we rewrite (2.13) as

$$\left[\frac{\partial^2}{\partial z^2}-\frac{\eta^2}{c^2}\frac{\partial^2}{\partial t^2}\right][\mathscr{E}_{Nn}(z,t)e^{i(k_{Nn}z-\omega_{Nn}t)}] = +i\chi\frac{4\pi}{c^2}\frac{\partial^2}{\partial t^2}\{[Q\mathscr{E}_{N,n+1}(z,t)e^{ik_{N,n+1}z} - Q^*\mathscr{E}_{N,n-1}(z,t)e^{ik_{N,n-1}z}]e^{-i\omega_{Nn}t}\} \,, \tag{2.14}$$

where η is the index of refraction of the medium, $\eta^2 \equiv 1+4\pi\chi$ and $k_{Nn} \equiv \eta\omega_{Nn}/c$. In order to be consistent with the equations derived for the material medium we make the slowly varying envelope and phase approximation (SVEPA) in the Maxwell equation, (2.14), i.e.,

$$|\mathscr{E}_{Nn}|\omega_{Nn} \gg \left|\frac{\partial\mathscr{E}_{Nn}}{\partial t}\right| \,, \tag{2.15a}$$

$$|\mathscr{E}_{Nn}|k_{Nn} \gg \left|\frac{\partial\mathscr{E}_{Nn}}{\partial z}\right| \,. \tag{2.15b}$$

To lowest order we find

$$\left[\frac{\partial}{\partial z}+\frac{1}{v^g_{Nn}}\frac{\partial}{\partial t}\right]\mathscr{E}_{Nn} = \left[\frac{4\pi M\mu^2}{\hbar c\omega_{01}\eta}\right]\omega_{Nn}(Q^*\mathscr{E}_{N,n-1}e^{i\Delta k_{N,n-1}z} - Q\mathscr{E}_{N,n+1}e^{-i\Delta k_{Nn}z}) \,, \tag{2.16}$$

where we have introduced the group velocity v^g_{Nn} in place of the constant velocity c/η. This substitution of the group velocity in (2.16) is the most important modification that we make in order to properly account for the frequency dependence of the linear susceptibility and the index of refraction. We explicitly calculate this result in the Appendix. The reason for this frequency dependence is the presence of other high-lying energy levels and the fact that ω_{01} is not infinitely large. The coefficient on the right side of (2.16) also suffers with respect to its precise frequency dependence for exactly the same reason. However, it is a much smaller effect and is ignored here. This derivation also neglects the population dependence and, therefore, the implicit time dependence of the index of refraction; however, this is consistent with the experimental conditions discussed in the next section.

III. ESSENTIAL PHYSICS

A. Simplification of equations

In order to study soliton formation analytically, so that we have a basis for understanding the "experimental"

simulations of the next section, we must further reduce equations (2.9) and (2.16). The approximations that we make are consistent with the experimental conditions: (1) $w \cong -1$ and (2) $\Delta k_{Nn} z_c \cong \Delta k_{Jj} z_c \ll \pi/2$, where z_c is the length of the cell. The first approximation means that we have many more molecules than photons, i.e., even if there is complete photon conversion from pump field to first-Stokes field, the molecular inversion which tracks the number of photons converted remains in the ground state. The second approximation means that the optical medium is short with respect to the frequency dependence of the index of refraction such that the field pairs' relative phases are equal and small. This approximation also implies that all the relative group velocities are equal and equal to v^g. The Maxwell-Bloch equations become

$$\dot{Q} = -\left[i(\Delta-\delta)+\frac{1}{T}\right]Q+\frac{\mu^2}{2\hbar^2\omega_{01}}\left[\sum_{N,n}\mathscr{E}_{Nn}\mathscr{E}^*_{N,n+1}\right], \tag{3.1a}$$

$$\left[\frac{\partial}{\partial z}+\frac{1}{v^g}\frac{\partial}{\partial t}\right]\mathscr{E}_{Nn} = \left[\frac{4\pi M\mu^2}{\hbar c\omega_{01}\eta}\right]\omega_{Nn}(Q^*\mathscr{E}_{N,n-1}-Q\mathscr{E}_{N,n+1}), \tag{3.1b}$$

where the w equation is eliminated by (1).

It is convenient to redefine the variables in (3.1) such that we have a system of units which is consistent with the experimental description of the process, i.e., intensity in MW/cm^2, frequency in cm^{-1}, time in ns, distance in cm, etc. Equations (3.1) become

$$\dot{Q} = -\left[i(\Delta-\delta)+\frac{1}{T}\right]Q+\sum_{N,n}\mathscr{E}_{Nn}\mathscr{E}^*_{N,n+1}, \tag{3.2a}$$

$$\left[\frac{\partial}{\partial z}+\frac{1}{v^g}\frac{\partial}{\partial t}\right]\mathscr{E}_{Nn} = \beta_N\frac{\omega_{Nn}}{\omega_{Ns}}(Q^*\mathscr{E}_{N,n-1}-Q\mathscr{E}_{N,n+1}), \tag{3.2b}$$

where ω_{Ns} refers to the frequency of the first-Stokes field in the Nth field chain, and β_N is related to the steady-state gain (G_N in cm/MW) of the first-Stokes field in the Nth field chain, $\beta_N \equiv G_N/T$. Obviously, $|\mathscr{E}_{Nn}|^2$ and Q are now in units of MW/cm^2 and mJ/cm^2, respectively.

By further specifying exact resonance, $\Delta=\delta$, and assuming real fields and, therefore, a real polarization, the equations now only will contain the most basic information necessary for studying soliton formation in four-wave mixing. In addition, it is useful to transform the variables z and t into a reference frame which is traveling with the fields at velocity v^g. Later it will be necessary to transform into a different reference frame, i.e., one which travels with the soliton at velocity v^s. Therefore, we transform (3.3) into a reference frame which is propagating at velocity v and choose this velocity to be either v^g or v^s depending on the circumstances. By defining a local time τ and space variable ξ, such that $\tau \equiv t - z/v$ and $\xi \equiv z$, we rewrite (3.2) in this new coordinate system:

$$\frac{\partial Q}{\partial \tau} = -\frac{Q}{T}+\sum_{N,n}\mathscr{E}_{Nn}\mathscr{E}_{N,n+1}, \tag{3.3a}$$

$$\left[\frac{\partial}{\partial \xi}+\left[\frac{1}{v^g}-\frac{1}{v}\right]\frac{\partial}{\partial \tau}\right]\mathscr{E}_{Nn} = \beta_N\frac{\omega_{Nn}}{\omega_{Ns}}Q(\mathscr{E}_{N,n-1}-\mathscr{E}_{N,n+1}), \tag{3.3b}$$

where

$$\frac{\partial}{\partial z} = -\frac{1}{v}\frac{\partial}{\partial \tau}+\frac{\partial}{\partial \xi}$$

and

$$\frac{\partial}{\partial \tau} = \frac{\partial}{\partial t}.$$

B. Method of solution

In this part of Sec. III we discuss a method of solving equations (3.3) which is valid independent of solitary wave generation and illustrates the basic physics of phase-matched transient four-wave-mixing processes. A related method was described by one of us (J.R.A.) several years ago for steady-state four-wave-mixing processes.[10]

It is convenient to first choose a local-time frame moving with the fields at velocity v^g, i.e., $v = v^g$. Equations (3.3) become

$$\frac{\partial Q}{\partial \tau} = -\frac{Q}{T}+\sum_{N,n}\mathscr{E}_{Nn}\mathscr{E}_{N,n+1}, \tag{3.4a}$$

$$\frac{\partial}{\partial \xi}\mathscr{E}_{Nn} = \beta_N\frac{\omega_{Nn}}{\omega_{Ns}}Q(\mathscr{E}_{N,n-1}-\mathscr{E}_{N,n+1}). \tag{3.4b}$$

We now define a new variable $\theta(\xi,\tau)$ such that all the fields $\mathscr{E}_{Nn}(\xi,\tau)$ depend on ξ through θ, i.e., $\mathscr{E}_{Nn}(\xi,\tau) \equiv \mathscr{E}_{Nn}(\theta,\tau)$. In addition, we define $\partial\theta/\partial\xi \equiv Q$. Using the chain rule for differentiation of $\mathscr{E}_{Nn}$ in (3.4b), noting the appearance of $\partial\theta/\partial\xi$ on both sides of this equation and canceling it, and substituting for Q in (3.4a) we obtain

$$\frac{\partial^2\theta}{\partial\tau\partial\xi} = -\frac{1}{T}\frac{\partial\theta}{\partial\xi}+\sum_{N,n}\mathscr{E}_{Nn}\mathscr{E}_{N,n+1}, \tag{3.5a}$$

$$\frac{\partial}{\partial\theta}\mathscr{E}_{Nn} = \beta_N\frac{\omega_{Nn}}{\omega_{Ns}}(\mathscr{E}_{N,n-1}-\mathscr{E}_{N,n+1}). \tag{3.5b}$$

Equations (3.5b) are linear first-order differential equations with constant coefficients in θ. For problems with a small number of fields the solutions are sine and cosine functions of θ. After finding these simple functions of θ and substituting them into (3.5a), the complete dynamics can be obtained by solving a single second-order partial differential equation for θ, (3.5a). Therefore, the physics of these phase-matched four-wave-mixing processes is determined by a single variable, $\theta(\xi,\tau)$, which translates the photon transfer dynamics of (3.5b) into real space-time dynamics.

C. Mathematical solitons

The type of solitons we will study in this section are those which are rigorous mathematical solutions to the equations of motion. In this sense these are not the solitons observed in the laboratory, but are local representa-

tions of the experimental observations. This will be easier to understand once we have reached Sec. IV.

Before considering specific examples of mathematical solitons, it is necessary to return to (3.3) and further reduce these equations. The first step is to go into a frame of reference which is moving with the soliton, $v=v^s$. If a soliton solution exists, then in this reference frame it must be independent of ξ, i.e., $(\partial/\partial\xi)\mathscr{E}_{Nn}=0$. The second step is to assume an infinite relaxation time, $T\to\infty$, which is consistent with the work of Chu and Scott on Raman solitons.[2] As was observed in the case of Raman scattering, these mathematical solutions can represent accurately, but only qualitatively, the local time dynamics of the electric field envelope in the vicinity of the soliton. This results because the relaxation time is finite. With these considerations in mind (3.3) becomes

$$\frac{\partial Q}{\partial\tau}=\sum_{N,n}\mathscr{E}_{Nn}\mathscr{E}_{N,n+1}\,, \tag{3.6a}$$

$$\frac{\partial}{\partial\tau}\mathscr{E}_{Nn}=-\gamma_N\frac{\omega_{Nn}}{\omega_{Ns}}Q(\mathscr{E}_{N,n-1}-\mathscr{E}_{N,n+1})\,, \tag{3.6b}$$

where $\gamma_N\equiv\beta_N/(1/v^s-1/v^g)$. Since the experimentally observed solitons propagate with a velocity $v^s<v^g$, the parameters γ_N are positive definite. Mathematical solitons exist for $v^s>v^g$, but we will not consider them here.

Following the procedure outlined in Sec. III B, we define a new variable $\theta(\tau)$ such that all the fields $\mathscr{E}_{Nn}(\tau)$ depend on τ through θ, i.e., $\mathscr{E}_{Nn}(\tau)\equiv\mathscr{E}_{Nn}(\theta)$. In addition, we define $\partial\theta/\partial\tau\equiv Q$. Using the chain rule for differentiation of $\mathscr{E}_{Nn}$ in (3.6b), noting the appearance of $\partial\theta/\partial\tau$ on both sides of this equation and canceling it, and substituting for Q in (3.6a) we find

$$\frac{\partial^2\theta}{\partial\tau^2}=\sum_{N,n}\mathscr{E}_{Nn}\mathscr{E}_{N,n+1}\,, \tag{3.7a}$$

$$\frac{\partial}{\partial\theta}\mathscr{E}_{Nn}=-\gamma_N\frac{\omega_{Nn}}{\omega_{Ns}}(\mathscr{E}_{N,n-1}-\mathscr{E}_{N,n+1})\,. \tag{3.7b}$$

Equations (3.7b), as with (3.5b), are linear first-order differential equations with constant coefficients in θ. Notice, however, the minus sign in (3.7b) as compared with (3.5b). It is just this minus sign which leads to the reversal of the "normal" time dynamics and the generation of the soliton. In the next three subsections we will study specific examples of four-wave-mixing solitons by solving (3.7b) for $\mathscr{E}_{Nn}(\theta)$, substituting these solutions into (3.7a), and solving (3.7a) for $\theta(\tau)$.

1. *Two-field case*

This first example of soliton generation corresponds to the case of stimulated Raman scattering studied originally by Chu and Scott.[2] We do this example only to illustrate the methodology.

Equations (3.7b) become

$$\frac{\partial}{\partial\theta}\mathscr{E}_{11}=\gamma_1\frac{\omega_{11}}{\omega_{12}}\mathscr{E}_{12}\,, \tag{3.8a}$$

$$\frac{\partial}{\partial\theta}\mathscr{E}_{12}=-\gamma_1\mathscr{E}_{11}\,, \tag{3.8b}$$

where $\mathscr{E}_{11}$ and $\mathscr{E}_{12}$ are the pump and first-Stokes fields, respectively. Since there is only one chain of fields in this example, we will, henceforth, omit the chain index, $N=1$. The essential physics of stimulated Raman scattering does not depend on the precise values of the field's frequencies, and, therefore, we set them equal, $\omega_1=\omega_2$. The solutions to (3.8) are

$$\mathscr{E}_1=\cos(\gamma\theta)\,, \tag{3.9a}$$

$$\mathscr{E}_2=-\sin(\gamma\theta)\,, \tag{3.9b}$$

where the total number of photons is normalized to unity, $\mathscr{E}_1^2+\mathscr{E}_2^2=1$.

Substituting (3.9) into (3.7a) gives

$$\frac{\partial^2\theta}{\partial\tau^2}=-\cos(\gamma\theta)\sin(\gamma\theta)=-\tfrac{1}{2}\sin(2\gamma\theta)\,, \tag{3.10}$$

which is a variant of the sine-Gordon equation. After multiplying both sides of the equation by $\partial\theta/\partial\tau$, we rewrite (3.10) as

$$\frac{1}{2}\frac{\partial}{\partial\tau}\left[\frac{\partial\theta}{\partial\tau}\right]^2=\frac{1}{4\gamma}\frac{\partial}{\partial\tau}\cos(2\gamma\theta)\,,$$

or

$$\left[\frac{\partial\theta}{\partial\tau}\right]^2=\frac{1}{2\gamma}[\cos(2\gamma\theta)+C]\,, \tag{3.11}$$

where C is the constant of integration. Choosing C equal to 1 and using a standard trigonometric identity we obtain

$$\frac{\partial\theta}{\partial\tau}=\pm\frac{1}{\sqrt{\gamma}}\cos(\gamma\theta)\,. \tag{3.12}$$

Upon choosing the + sign and integrating (3.12) with the appropriate boundary conditions we find that $\sin(\gamma\theta)=\tanh(\sqrt{\gamma}\tau)$, i.e., (3.9) becomes

$$\mathscr{E}_1=\operatorname{sech}(\sqrt{\gamma}\tau)\,, \tag{3.13a}$$

$$\mathscr{E}_2=-\tanh(\sqrt{\gamma}\tau)\,, \tag{3.13b}$$

where $-\pi/2\le\gamma\theta\le\pi/2$ and $-\infty\le\tau\le\infty$, respectively. The solution for Q is easily found from (3.12),

$$Q=\frac{1}{\sqrt{\gamma}}\operatorname{sech}(\sqrt{\gamma}\tau)\,. \tag{3.14}$$

Obviously, $\sqrt{\gamma}$ is proportional to the inverse of the width of the soliton which means by increasing the gain or by making v^s closer to v^g the soliton narrows.

In Fig. 2(a) we plot the pump amplitude $\mathscr{E}_1$ and first-

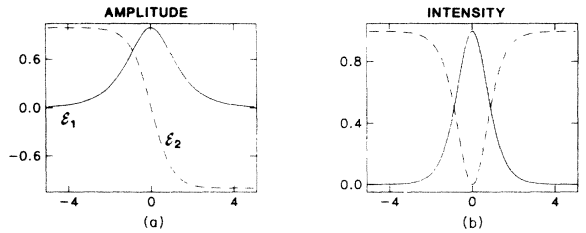

FIG. 2. Raman soliton, pump field is $\mathscr{E}_1$, first-Stokes field is $\mathscr{E}_2$, (a) amplitude and (b) intensity.

Stokes amplitude $\mathscr{E}_2$ versus τ using (3.8) with $\gamma=1$. Figure 2(b) is the same as Fig. 2(a), except we plot the fields' intensities, $\mathscr{E}_1^2$ and $\mathscr{E}_2^2$. Looking at Fig. 2(a) we see that this two-field soliton represents the appearance of pump photons and the corresponding absence of first-Stokes photons. At the point the pump is a maximum we observe a sign flip in the electric field envelope of the first-Stokes field. It is this sign flip which originally inspired Drühl to insert a π phase change into the first-Stokes seed in his computer model.

2. *Three-field case*

In Fig. 3 we show two types of three-field problems. Figure 3(a) shows anti-Stokes scattering where the first-anti-Stokes field, the pump field, and the first-Stokes field in our notation are $\mathscr{E}_1$, $\mathscr{E}_2$, and $\mathscr{E}_3$, respectively. Figure 3(b) shows second-Stokes generation where the pump field, the first-Stokes field, and the second-Stokes field are in this case $\mathscr{E}_1$, $\mathscr{E}_2$, and $\mathscr{E}_3$, respectively. We have neglected the chain index here, as it is superfluous. Mathematically the only difference between these two problems is in the choice of parameters and in the initial conditions. Therefore, the method of solution for these two problems is the same.

Equations (3.7b) for this case become

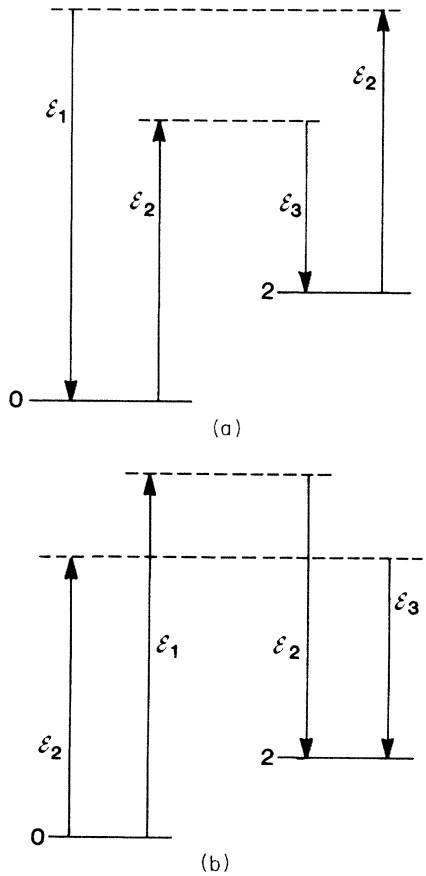

FIG. 3. Three-field models, (a) anti-Stokes scattering, (b) second-Stokes generation.

$$\frac{\partial}{\partial\theta}\mathscr{E}_1=\gamma\mathscr{E}_2\,, \tag{3.15a}$$

$$\frac{\partial}{\partial\theta}\mathscr{E}_2=\gamma(\mathscr{E}_3-\mathscr{E}_1)\,, \tag{3.15b}$$

$$\frac{\partial}{\partial\theta}\mathscr{E}_3=-\gamma\mathscr{E}_2\,, \tag{3.15c}$$

where we have set $\gamma_1=\gamma$ and $\omega_1=\omega_2=\omega_3$. The essential physics of these two examples is not influenced by these restrictions. One solution to (3.15) is

$$\mathscr{E}_1=\frac{1+\cos(\sqrt{2}\gamma\theta)}{2}=\cos^2\left[\frac{\gamma\theta}{\sqrt{2}}\right], \tag{3.16a}$$

$$\mathscr{E}_2=-\frac{\sin(\sqrt{2}\gamma\theta)}{\sqrt{2}}=-\sqrt{2}\cos\left[\frac{\gamma\theta}{\sqrt{2}}\right]\sin\left[\frac{\gamma\theta}{\sqrt{2}}\right], \tag{3.16b}$$

$$\mathscr{E}_3=\frac{1-\cos(\sqrt{2}\gamma\theta)}{2}=\sin^2\left[\frac{\gamma\theta}{\sqrt{2}}\right], \tag{3.16c}$$

where we have normalized the total number of photons to unity, $\mathscr{E}_1^2+\mathscr{E}_2^2+\mathscr{E}_3^2=1$. The other free parameter, which must be specified in order to have the unique solution, has been chosen such that the source term in (3.7a) is maximized. Another solution to (3.15) will be studied later in this section.

Substituting (3.16) into (3.7a) gives

$$\frac{\partial^2\theta}{\partial\tau^2}=-\frac{\sin(\sqrt{2}\gamma\theta)}{\sqrt{2}}\,, \tag{3.17}$$

which like (3.10) is a variant of the sine-Gordon equation. If we let $\sqrt{2}\theta\rightarrow 2\Phi$ in (3.17), then (3.17) becomes identical with (3.10). Following the same procedure as was done in the previous example, we find in this case $\sin(\gamma\theta/\sqrt{2})=\tanh(\sqrt{\gamma}\tau)$, i.e., (3.16) becomes

$$\mathscr{E}_1=\operatorname{sech}^2(\sqrt{\gamma}\tau)\,, \tag{3.18a}$$

$$\mathscr{E}_2=-\sqrt{2}\operatorname{sech}(\sqrt{\gamma}\tau)\tanh(\sqrt{\gamma}\tau)\,, \tag{3.18b}$$

$$\mathscr{E}_3=\tanh^2(\sqrt{\gamma}\tau)\,, \tag{3.18c}$$

where $-\pi/2\leq\gamma\theta/\sqrt{2}\leq\pi/2$ and $-\infty\leq\tau\leq\infty$, respectively. The solution for Q is

$$Q=\sqrt{2/\gamma}\operatorname{sech}(\sqrt{\gamma}\tau)\,. \tag{3.19}$$

In Fig. 4(a) we plot the amplitudes $\mathscr{E}_1$, $\mathscr{E}_2$, and $\mathscr{E}_3$ versus τ using (3.18) with $\gamma=1$. Figure 4(b) is the same as Fig. 4(a), except we plot the fields' intensities, $\mathscr{E}_1^2$, $\mathscr{E}_2^2$, and $\mathscr{E}_3^2$. Looking at Fig. 4(a) we see that this three-field soliton represents the appearance of $\mathscr{E}_1$ photons at the expense of $\mathscr{E}_3$ photons. $\mathscr{E}_2$ photons appear in the interchange regions where $\mathscr{E}_1$ and $\mathscr{E}_3$ photons are being exchanged. At the point of maximum $\mathscr{E}_1$ or minimum $\mathscr{E}_3$ the field $\mathscr{E}_2$ undergoes a sign reversal. One may be able to generate this three-field soliton by inserting a π phase flip into the field $\mathscr{E}_2$.

Another solution to (3.15) is

$$\mathscr{E}_1=-\frac{\cos(\sqrt{2}\gamma\theta)}{\sqrt{2}}\,, \tag{3.20a}$$

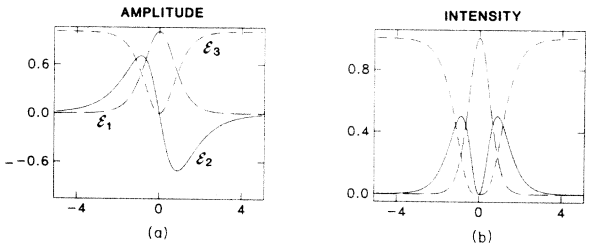

FIG. 4. Three-field soliton consistent with second-Stokes generation, i.e., pump field is $\mathscr{E}_1$, first-Stokes field is $\mathscr{E}_2$, second-Stokes field is $\mathscr{E}_3$, (a) amplitude and (b) intensity.

$$\mathscr{E}_2=\sin(\sqrt{2}\gamma\theta)\ , \tag{3.20b}$$

$$\mathscr{E}_3=\frac{\cos(\sqrt{2}\gamma\theta)}{\sqrt{2}}\ , \tag{3.20c}$$

where the total number of photons is normalized to unity. The second free parameter has been chosen such that the source term in (3.7a) is a minimum, and the solution is nontrivial.

Substituting (3.20) into (3.7a) gives

$$\frac{\partial^2\theta}{\partial\tau^2}=0\ . \tag{3.21}$$

The solution to (3.21) in this case is $\sqrt{2}\gamma\theta=k\tau$, i.e., Eqs. (3.20) become

$$\mathscr{E}_1=-\frac{\cos(k\tau)}{\sqrt{2}}\ , \tag{3.22a}$$

$$\mathscr{E}_2=\sin(k\tau)\ , \tag{3.22b}$$

$$\mathscr{E}_3=\frac{\cos(k\tau)}{\sqrt{2}}\ , \tag{3.22c}$$

where $0\le\sqrt{2}\gamma\theta\le\pi$ and $0\le k\tau\le\pi$, respectively. The solution for Q is $Q=k/\sqrt{2}\gamma$, a constant. The width of the solution (3.22) is independent of both the gain and the velocity v^s.

In Fig. 5(a) we plot the amplitudes $\mathscr{E}_1$, $\mathscr{E}_2$, and $\mathscr{E}_3$ versus τ using (3.22) with $k=1$. Figure 5(b) is the same as Fig. 5(a), except we plot the fields' intensities, $\mathscr{E}_1^2$, $\mathscr{E}_2^2$, and $\mathscr{E}_3^2$. Looking at Fig. 5(a) we observe that at $\tau=\pi/2$ the first and third fields undergo a π phase change. Therefore, it may be possible to generate this soliton by introducing a π phase change into either or both $\mathscr{E}_1$ and $\mathscr{E}_3$.

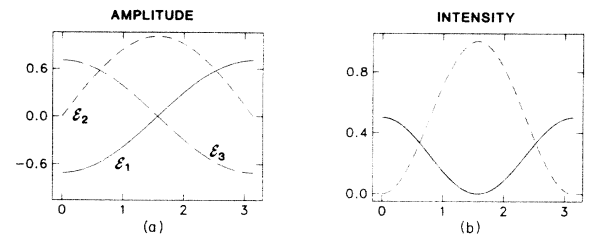

FIG. 5. Three-field soliton consistent with anti-Stokes scattering, i.e., anti-Stokes field is $\mathscr{E}_1$, pump field is $\mathscr{E}_2$, first-Stokes field is $\mathscr{E}_3$, (a) amplitude and (b) intensity.

3. *Two-pump four-field case*

In Fig. 6 we show an example of four-wave mixing where there are two pump fields present. Both pumps can generate only their respective first-Stokes fields.

Equations (3.7b) for this case are

$$\frac{\partial}{\partial\theta}\mathscr{E}_{11}=\gamma_1\frac{\omega_{11}}{\omega_{12}}\mathscr{E}_{12}\ , \tag{3.23a}$$

$$\frac{\partial}{\partial\theta}\mathscr{E}_{12}=-\gamma_1\mathscr{E}_{11}\ , \tag{3.23b}$$

$$\frac{\partial}{\partial\theta}\mathscr{E}_{21}=\gamma_2\frac{\omega_{21}}{\omega_{22}}\mathscr{E}_{22}\ , \tag{3.23c}$$

$$\frac{\partial}{\partial\theta}\mathscr{E}_{22}=-\gamma_2\mathscr{E}_{21}\ , \tag{3.23d}$$

where there are a limited number of ways for choosing parameters in (3.23) so that analytic solutions are obtained. We set $\omega_{11}=\omega_{12}$ and $\omega_{21}=\omega_{22}$. In addition, we choose the gain for chain 1 to be twice the gain for chain 2, $\gamma_1=2\gamma_2\equiv2\gamma$, and the intensity for chain 1 to be half the intensity for chain 2, $\mathscr{E}_{11}^2+\mathscr{E}_{12}^2=\frac{1}{2}$ and $\mathscr{E}_{21}^2+\mathscr{E}_{22}^2=1$. The solutions to (3.23) are

$$\mathscr{E}_{11}=\frac{\cos(2\gamma\theta)}{\sqrt{2}}\ , \tag{3.24a}$$

$$\mathscr{E}_{12}=-\frac{\sin(2\gamma\theta)}{\sqrt{2}}\ , \tag{3.24b}$$

$$\mathscr{E}_{21}=\cos(\gamma\theta)\ , \tag{3.24c}$$

$$\mathscr{E}_{22}=-\sin(\gamma\theta)\ . \tag{3.24d}$$

Substituting (3.24) into (3.7a) gives

$$\begin{aligned}\frac{\partial^2\theta}{\partial\tau^2}&=-\frac{\cos(2\gamma\theta)\sin(2\gamma\theta)}{2}-\sin(\gamma\theta)\cos(\gamma\theta)\\&=-\frac{\cos(2\gamma\theta)\sin(2\gamma\theta)}{2}-\frac{\sin(2\gamma\theta)}{2}\\&=-\frac{\sin(4\gamma\theta)}{4}-\frac{\sin(2\gamma\theta)}{2}\ ,\end{aligned} \tag{3.25}$$

which is a variant of the double sine-Gordon equation. After multiplying both sides of the equation by $\partial\theta/\partial\tau$

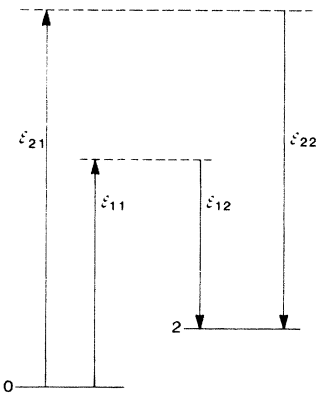

FIG. 6. Two-pump four-field model.

and using the middle form of (3.25), we rewrite (3.25) as

$$\frac{1}{2}\frac{\partial}{\partial\tau}\left[\frac{\partial\theta}{\partial\tau}\right]^2=\frac{1}{8\gamma}\frac{\partial}{\partial\tau}[\cos^2(2\gamma\theta)+2\cos(2\gamma\theta)]\ ,$$

or (3.26)

$$\left[\frac{\partial\theta}{\partial\tau}\right]^2=\frac{1}{4\gamma}[\cos^2(2\gamma\theta)+2\cos(2\gamma\theta)+C]\ ,$$

where C is the constant of integration. Choosing C equal to 1 and using a standard trigonometric identity we obtain

$$\frac{\partial\theta}{\partial\tau}=\pm\frac{1}{\sqrt{\gamma}}\cos^2(\gamma\theta)\ . \tag{3.27}$$

Upon choosing the + sign and integrating (3.27) with the appropriate boundary conditions we find that $\tan(\gamma\theta)=\sqrt{\gamma}\tau$, i.e., using standard trigonometric identities (3.27) becomes

$$\mathscr{E}_{11}=\frac{1}{\sqrt{2}}\left[\frac{1-\gamma\tau^2}{1+\gamma\tau^2}\right]\ , \tag{3.28a}$$

$$\mathscr{E}_{12}=-\frac{1}{\sqrt{2}}\left[\frac{2\sqrt{\gamma}\tau}{1+\gamma\tau^2}\right]\ , \tag{3.28b}$$

$$\mathscr{E}_{21}=\frac{1}{(1+\gamma\tau^2)^{1/2}}\ , \tag{3.28c}$$

$$\mathscr{E}_{22}=-\frac{\sqrt{\gamma}\tau}{(1+\gamma\tau^2)^{1/2}}\ , \tag{3.28d}$$

where $-\pi/2\le\gamma\theta\le\pi/2$ and $-\infty\le\tau\le\infty$, respectively. The solution for Q is

$$Q=\frac{1}{\sqrt{\gamma}}\left[\frac{1}{1+\gamma\tau^2}\right]\ . \tag{3.29}$$

In Fig. 7(a) we plot the amplitudes $\mathscr{E}_{11}$ and $\mathscr{E}_{12}$ versus τ using (3.28) with $\gamma=1$. Figure 7(b) is the same as Fig. 7(a), except we plot the fields' intensities, $\mathscr{E}_{11}^2$ and $\mathscr{E}_{12}^2$.

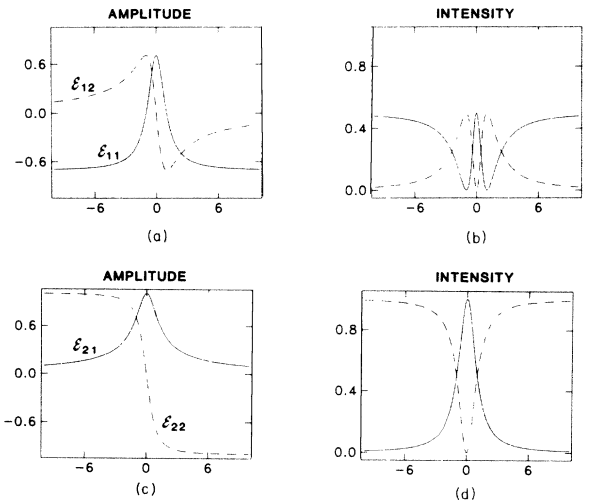

FIG. 7. Two-pump four-field soliton, pump_1 field is $\mathscr{E}_{11}$, first-Stokes_1 field is $\mathscr{E}_{12}$, pump_2 field is $\mathscr{E}_{21}$, first-Stokes_2 field is $\mathscr{E}_{22}$, (a) field pair_1 amplitude and (b) intensity, (c) field pair_2 amplitude and (d) intensity.

Figures 7(c) and 7(d) are the same as 7(a) and 7(b), except for $\mathscr{E}_{21}$ and $\mathscr{E}_{22}$. Looking at Figs. 7(c) and 7(d) we observe that the soliton for these fields is similar to the two-field soliton shown in Fig. 2. In this case, however, the shape of the fields is Lorentzian, and, therefore, much broader. In Figs. 7(a) and 7(b) we see very different Lorentzian type soliton structures. The pump field in this case is initially a maximum with the first-Stokes field, zero. The pump field in time then proceeds to deplete to zero, undergo a π phase shift and return to a maximum at the halfway point. During this time period the first-Stokes field builds from zero to a maximum, corresponding to the zero in the pump, and returns to zero as the pump returns to a maximum at the halfway point. The first-Stokes field undergoes a π phase shift at the halfway point. As we proceed from the halfway point to positive infinity, both fields reverse their time dynamics, with the pump symmetric and the first-Stokes antisymmetric. Since in this case there are several π phase shifts, it is not clear how to experimentally generate this soliton.

Before concluding this section we would like to point out that these examples of four-wave-mixing solitons are not the only cases which exhibit analytic solutions. There are actually many others. However, like the last case they may require very special parameter choices. In practice it is possible to choose more realistic parameters and still obtain solitons, but (3.7a) probably will require numerical integration. It is also possible that soliton solutions may not exist for certain parameter values.

In the next section we will consider the potential for experimentally generating the solitons discussed here using the technique of introducing a π phase shift into the electric field envelopes. We will numerically simulate experiments by integrating equations (3.4).

IV. "EXPERIMENTAL" SIMULATIONS

In this section we numerically study the solitons derived in Sec. III C. Our computations will use the technique of introducing a π phase shift in one or more of the input fields in order to generate a soliton structure. Since in real experiments the relaxation time of the polarization is finite, not infinite as assumed in Sec. III C, we will set $T=1$ ns. In all cases the frequencies will be set equal.

Our pulses in time will be super-Gaussian such that they appear relatively square. The full width at half maximum (FWHM) of the pulses will be roughly 20 ns. When a π phase shift is introduced in a pulse envelope, it will be introduced at the center, except for the two-pump two-field case. We will view the fields in a reference frame moving with $v=v^g$ such that the solitons are delayed relative to the rest of the pulse envelope as viewed at the cell exit. The input pump energy will be 20 mJ/cm^2 so that the input pump intensity is roughly 1 MW/cm^2. The input first-Stokes energy will be three orders of magnitude smaller than the pump. The gain will be chosen individually for each case such that the pulses' central temporal region shows sufficient photon conversion to be consistent with soliton input conditions. The cell length will be 3 ns.

The figures in this section will show each pulse's tem-

poral intensity profile at input to the cell and at output from the cell versus local pulse time τ. Superimposed on these figures will be the phase of the electric field envelope versus τ where zero radians is in the center, 2π radians very close to the top, and -2π radians very close to the bottom of the rectangular viewing area. Since the electric fields are real, we will only observe zero and $\pm\pi$.

A. Stimulated Raman scattering (two-field case)

For this example we have a pump and first-Stokes field. The temporal intensity profiles at input to the Raman cell are shown in Figs. 8(a) and 8(b). Notice the phase of both fields is zero. In Figs. 8(c) and 8(d) we show the intensity profiles at output from the Raman cell. Our choice of parameters gives very strong pump depletion. The asymmetry in the pump field is due to the finite relaxation time of the medium. If the relaxation time were infinite, then the output fields would be symmetric. The output fields' phases are zero. This type of output was typically observed experimentally by Wenzel and Carlsten.

In Figs. 9(a) and 9(b) we show the intensity profiles at the input to the Raman cell where we have now introduced an instantaneous π phase shift in the Stokes electric field envelope. In Figs. 9(c) and 9(d) we show the intensity profiles at the output from the Raman cell. The spike in the output pump field and corresponding dip in the output Stokes field represents the induced soliton structure. This soliton should be compared with the mathematical soliton shown in Fig. 2. Notice the relative location of the Stokes phase shift on input and output. This difference corresponds to the slower velocity of the soliton relative to the fields' group velocity. Due to the finiteness of the relaxation time, the shape of the soliton structure is not of the form given in Sec. III C 1. It is structures like these that were observed by Wenzel and Carlsten randomly and rarely in their original experiments. In comparing Figs. 8 and 9, one observes that the

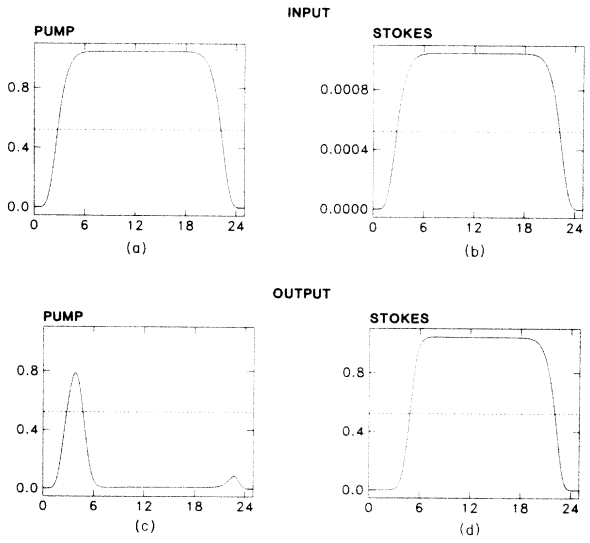

FIG. 8. Raman scattering input temporal intensity profiles, (a) pump, (b) first-Stokes, (c) and (d) are the corresponding output temporal intensity profiles. Horizontal axes are time (ns) and vertical axes are intensity (MW/cm^2).

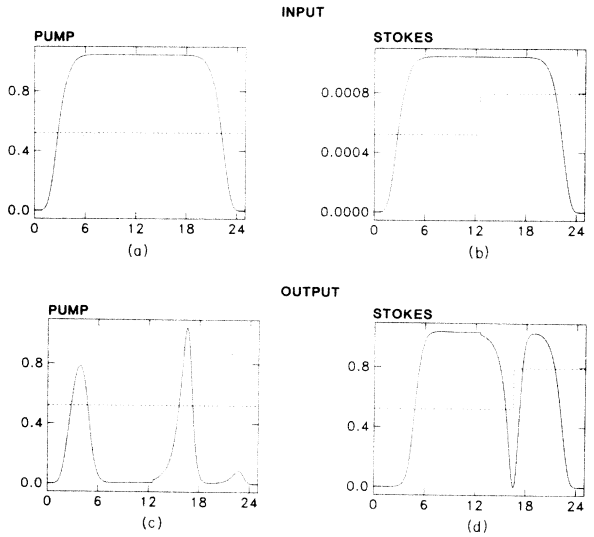

FIG. 9. Same as Fig. 8, except the input first-Stokes field has an instantaneous π phase shift introduced into its electric field envelope.

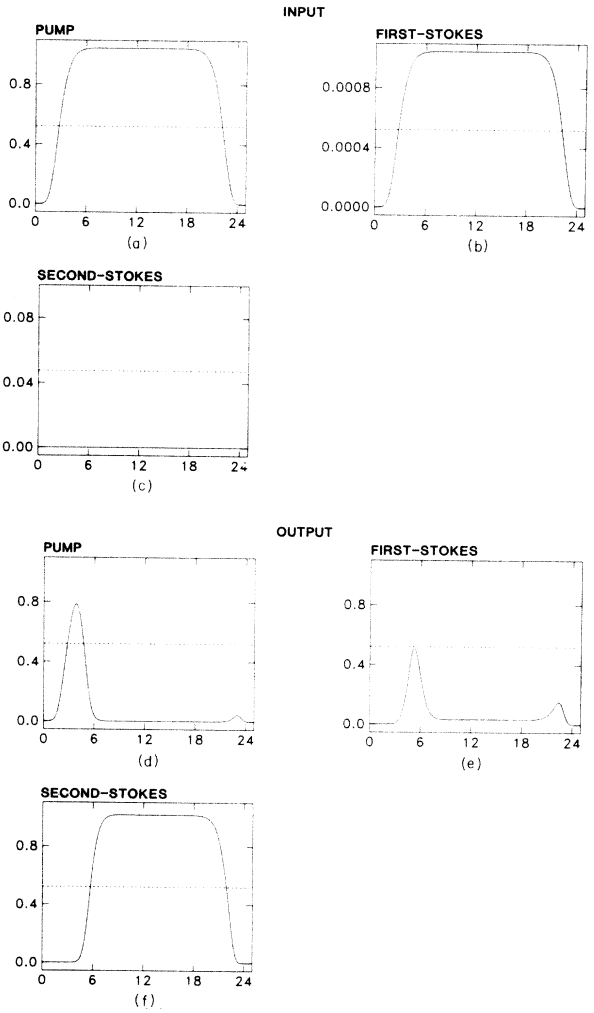

FIG. 10. Second-Stokes generation input temporal intensity profiles, (a) pump, (b) first-Stokes, (c) second-Stokes, (d)—(f) are corresponding output temporal intensity profiles. Axes are the same as in Fig. 8.

intensity of the output fields in the two cases only differs by the soliton structure, all other features remain unchanged.

B. Second-Stokes generation (three-field case)

We consider normal second-Stokes generation first, i.e., all the input fields have the same phase, zero. Initially, we will set the input second-Stokes field to zero which forces it to arise entirely from four-wave mixing. In Figs. 10(a)—10(c) we show the input temporal intensity profiles of the pump, first-Stokes, and second-Stokes fields temporal profiles, respectively. In Figs. 10(d)—10(f) we show the same fields at the output from the cell. The gain has been chosen such that the pump and first-Stokes fields are strongly depleted. The transiency results in very asymmetric temporal profiles.

Referring back to Fig. 4, we observe that the input conditions for this soliton are depleted fields one and two and an undepleted field three, which is consistent with Figs. 10(d)—10(f). In addition, we observe that it is the second field which undergoes a sign change at the center of the soliton. Therefore, we introduce an instantaneous π phase shift in the first-Stokes field. In Figs. 11(a)—11(c) we show the input fields' temporal profiles. In Figs. 11(d)—11(f) we show the corresponding output fields. Comparing the location of the first-Stokes phase change on input and output shows a delay in the soliton with respect to the body of the pulse. Comparing the differences in the fields between Figs. 10 and 11 gives the features representative of the soliton. The second field shows a two-spike structure whereas the first and third fields show a spike and dip, respectively. The spike in the first field is narrower than the dip in the third field. These features are all consistent with Fig. 4(b). Both Wenzel and Carlsten plan to look for this soliton in the near future.[7]

C. Stimulated anti-Stokes scattering (three-field case)

In order to study "normal" anti-Stokes scattering we set all the initial phases to zero. In addition, we set the anti-Stokes field intensity initially to zero forcing it to arise solely from four-wave mixing. In Figs. 12(a)—12(c) we show the input fields' temporal profiles where the first

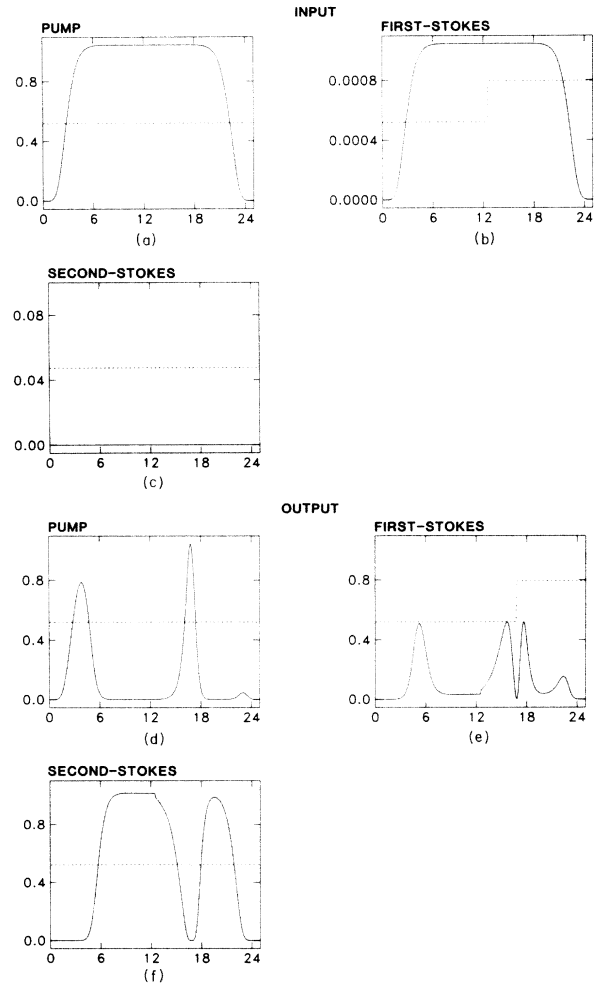

FIG. 11. Same as Fig. 10 except the input first-Stokes field has an instantaneous π phase shift introduced into its electric field envelope.

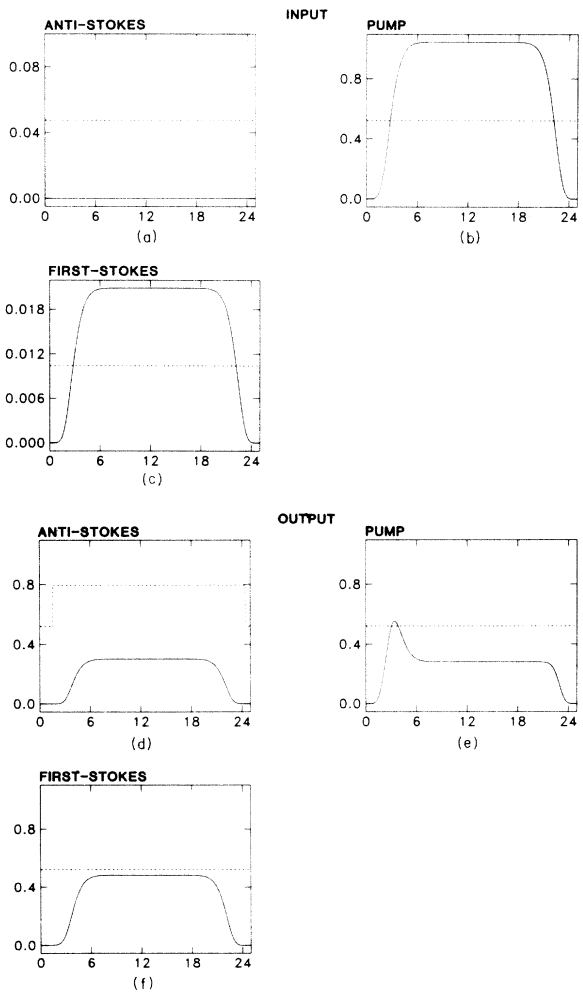

FIG. 12. Anti-Stokes scattering input temporal intensity profiles, (a) anti-Stokes, (b) pump, (c) first-Stokes, (d)—(f) are the corresponding output temporal intensity profiles. Axes are the same as in Fig. 8.

field is the anti-Stokes field; the second field is the pump field, and the third field is the first-Stokes field. In Figs. 12(d)—12(f) we show the output fields, respectively. Because of our initial conditions and parameter choices, we are able to generate a significant amount of anti-Stokes before the phase matching halts the on-axis forward conversion.[11] Due to the transiency there is some asymmetric conversion easily visible in the first-Stokes field. Note also that the phase of the output anti-Stokes field is shifted by π relative to the other fields.

The soliton illustrated in Fig. 5 shows that the first and third fields have equal intensity initially and that the second field is depleted initially. The first field is π out of phase with the third field. These initial conditions are consistent with Fig. 12, even though they are not exactly the same. Since initially we do not have any anti-Stokes photons, we will insert an instantaneous π phase shift into the third field, the first-Stokes, and see if we can induce the solitary wave structure. In Figs. 13(a)—13(c) we show the input temporal profiles. In Figs. 13(d)—13(f) we show the output temporal profiles. Comparing Figs. 12 and 13 enables us to distinguish the features of the soliton. Comparing the input and output first-Stokes' phase shift in Fig. 13 shows that the velocity delay of the soliton is very

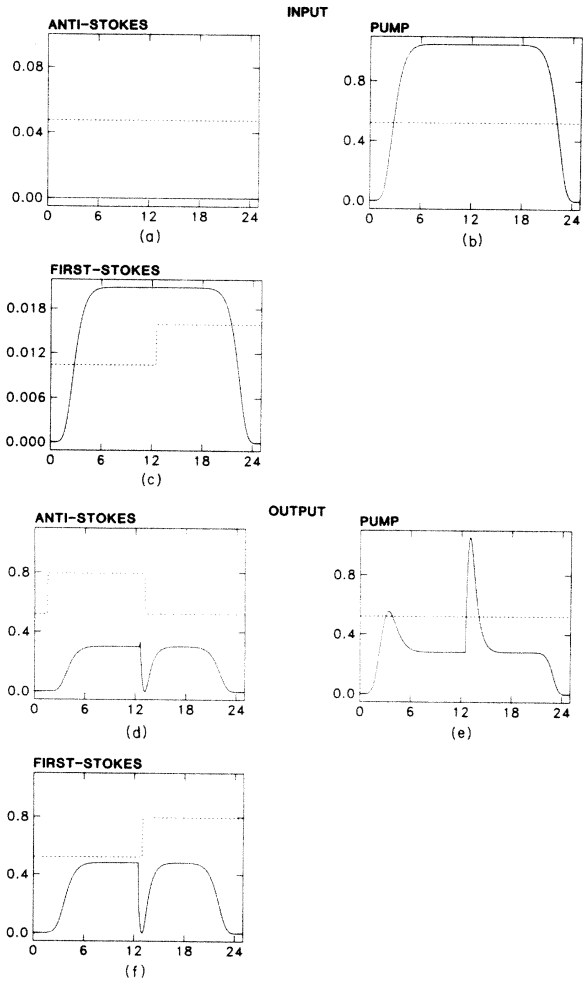

FIG. 13. Same as Fig. 12, except the input first-Stokes field has an instantaneous π phase shift introduced into its electric field envelope.

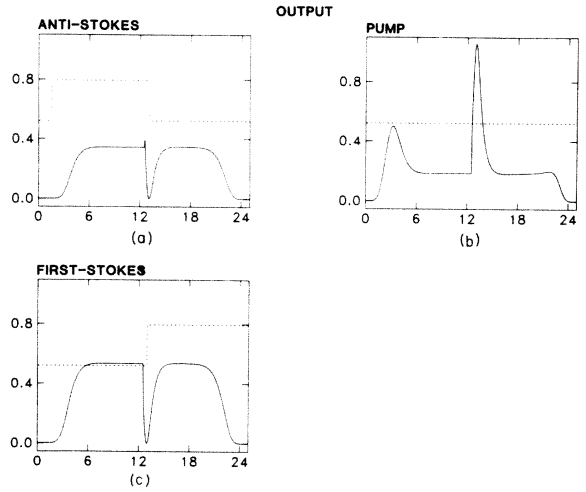

FIG. 14. (a)—(c) are the same as in Fig. 13(d)—13(f), except the gain has been increased.

small. In addition, we see that the phase of the first and third fields on output from the cell are now consistent with Fig. 5. In Sec. III C 2 we found that this soliton was independent of γ and, therefore, independent of v^s and the gain. In order to test the insensitivity of the soliton to gain we repropagated the fields, but with the gain significantly increased. The results are shown in Figs. 14(a)—14(c) where we observe only a slight increase in the conversion efficiency and no substantial change in the soliton. Since the relaxation time from a physical standpoint must play an important role in the rise and fall of the soliton, we again repropagated the fields, but with the relaxation time doubled. In Figs. 15(a)—15(c) we show the numerical results for the output temporal profiles. We observe a doubling of the soliton width.

D. Two-pump conversion (four-field case)

We will correlate this simulation to that studied in Sec. III C 3 by choosing the input field intensities such that the

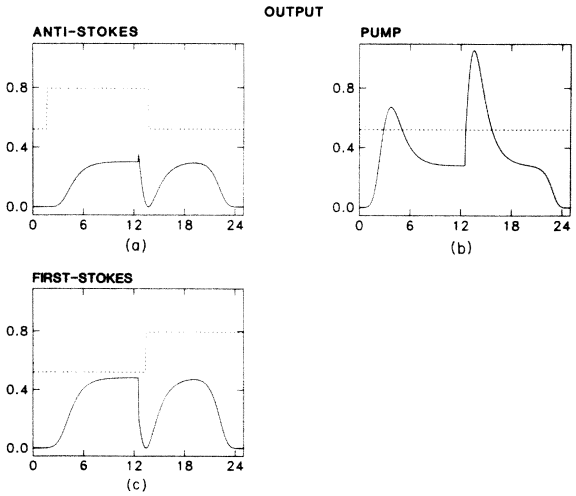

FIG. 15. (a)—(c) are the same as in Fig. 13(d)—13(f), except the relaxation time has been doubled.

first pair has half the intensity of the second pair. The gain for the first pair will be twice that for the second pair. Normal Raman scattering for this case will occur when all the input phases are zero. In Figs. 16(a)—16(d) we show these input fields' temporal profiles. Figures 16(a) and 16(b) correspond to the pump and first-Stokes of the first field pair, and Figs. 16(c) and 16(d) to the same fields for the second field pair, respectively. In Figs. 16(e)—16(h) we show the corresponding output fields. The gain has been chosen such that the second field pair is in the normal depletion regime. The first field pair is in a reverse regime where the first-Stokes is returning photons to the pump field, after having gone through the normal depletion regime earlier in the cell. The asymmetry in the fields' envelopes is due to the transiency of the medium. One should also notice that the phase of the first pump is π out of phase with the other fields.

Referring back to the soliton structure shown in Fig. 7, we observe that the output temporal profiles shown in Figs. 16 are consistent with this soliton's initial conditions. The first field pair has an undepleted pump field and depleted first-Stokes field with the phase of the pump at π. The second field pair has a depleted pump field and undepleted first-Stokes field of the same zero phase. In order to generate the soliton shown in Fig. 7 we will introduce a π phase shift into the first-Stokes field of the second field pair. Since the soliton structure found in Sec. III C 3 is a Lorentzian and, therefore, very broad, we will introduce the π phase shift earlier in the temporal pulse envelope than in the previous cases. In Figs. 17(a)—17(d) we show the input temporal profiles. In Figs. 17(e)—17(h) we show the output temporal profiles. Comparing Figs. 16 and 17 enables us to observe the soliton structure and identify it as that shown in Fig. 7. The structures observed are broader for the second field pair as compared with those for the first field pair. Comparing the phase shift on input and output for the first-Stokes field of the second field pair, we observe a substantial delay in the soliton. We believe that this single π phase shift was successful in generating this complex soliton structure because it is the only π phase shift which is consistent with the initial conditions at the cell input.

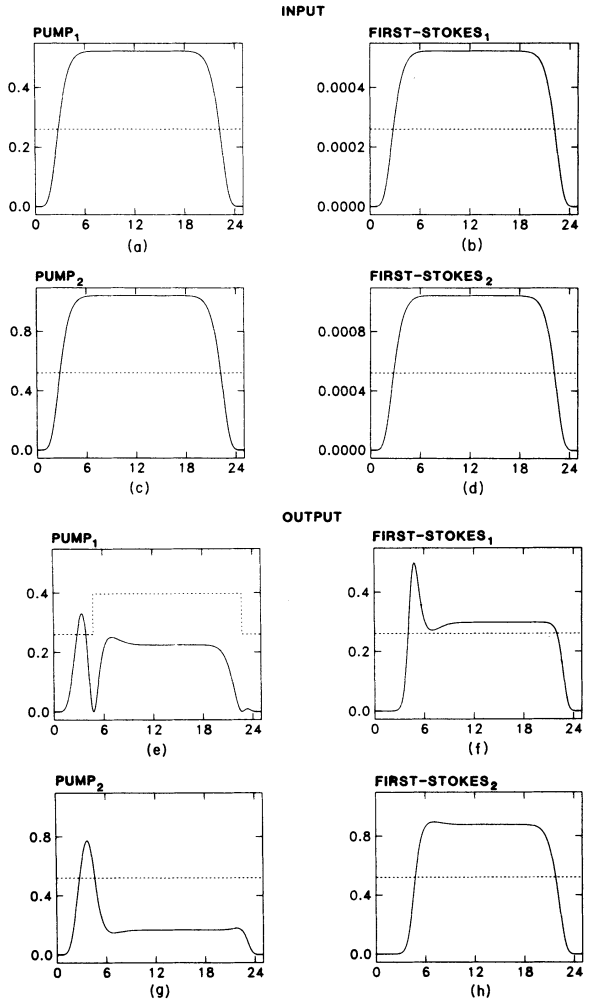

FIG. 16. Two-pump Raman scattering input temporal intensity profiles, (a) pump_1, (b) first-Stokes_1, (c) pump_2, (d) first-Stokes_2, (e)—(h) are the corresponding output temporal intensity profiles. Axes are the same as in Fig. 8.

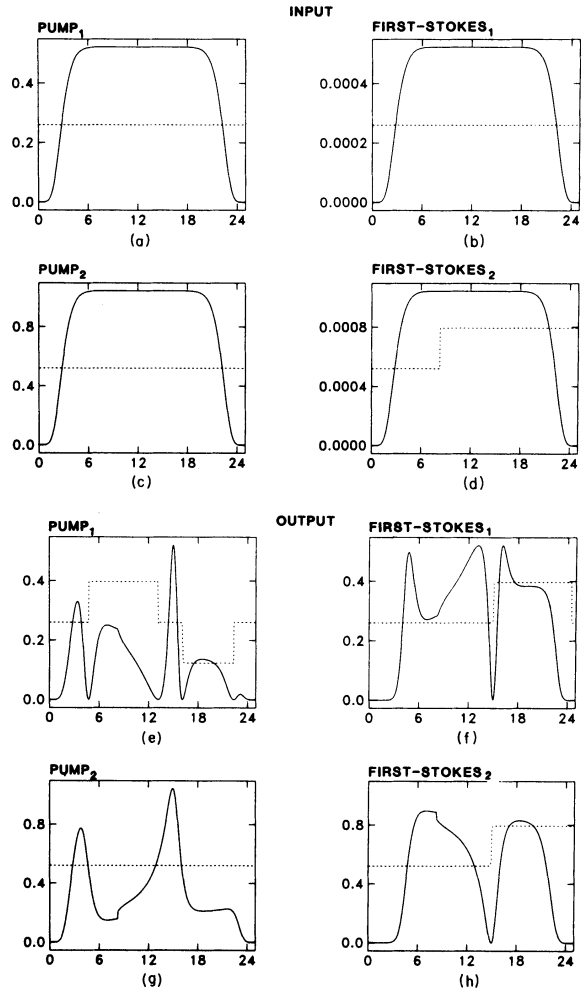

FIG. 17. Same as Fig. 16, except the input first-Stokes field of the second field pair has an instantaneous π phase shift introduced into its electric field envelope.

V. SUMMARY

In Sec. III we showed several examples of mathematical soliton solutions for two-, three-, and four-field problems. These analytic solutions demonstrated the potential richness for solitary wave generation in four-wave mixing problems in a Raman medium. We specifically discussed the problems of anti-Stokes scattering, second-Stokes generation, and two-pump Raman scattering. We believe that there are many other four-wave-mixing problems which can exhibit solitary wave formation.

While our parameter choices are artificial, it should be clear to the reader that realistic parameter choices for similar types of problems will lead to solitary wave generation. The exact form of these solitons, however, requires numerical simulation, but should be closely related to the solutions found here.

The technique of introducing instantaneous π phase shifts in particular input fields was shown to lead in all cases to stimulated scattering phenomena closely related to the analytic solutions. This technique is accessible both to the theorist and the experimentalist.

We look forward in the future to seeing real experiments demonstrating these or other solitons using the physics of four-wave mixing in Raman type media. More realistic numerical simulations of these experiments will expand our knowledge of this subject.

Note added in proof. The term soliton has historically been used for these wave structures observed in Raman scattering, and we have used this terminology here. In the earlier examples and in our more general four-wave mixing case, we believe the term "solitary wave" is more appropriate, although we have used the terms soliton and solitary wave interchangeably in the text.

ACKNOWLEDGMENTS

The authors express their thanks to John Carlsten, Bob Wenzel, Norman Kurnit, Mike Raymer, Paul Berman, and Kai Drühl for many useful and valuable discussions. P.W.M. acknowledges the support of the National Science Foundation through Grant No. PHY-8418070 at the University of Arkansas.

APPENDIX

In this appendix we show the relationship between the SVEPA and the group velocity in Maxwell's equations. These results are well known to researchers whose work involves propagation in optical fibers or other highly dispersive media.[6,12–15] However, since we have noticed that many researchers do not distinguish n/c and v^g in the Raman scattering literature, this seemed to be an appropriate forum to illustrate a simple derivation of the proper result.

We first expand any electric field and its generated polarization in terms of their frequency components:

$$E(z,t)=\sum_l \mathscr{E}_l e^{i[(k_l-k)z-(\omega_l-\omega)t]}e^{i(kz-\omega t)} \equiv \mathscr{E}(z,t)e^{i(kz-\omega t)} , \tag{A1}$$

$$P(z,t)=\sum_l \chi(\omega_l)\mathscr{E}_l e^{i[(k_l-k)z-(\omega_l-\omega)t]}e^{i(kz-\omega t)} \equiv p(z,t)e^{i(kz-\omega t)} , \tag{A2}$$

where $\mathscr{E}$ and p are slowly varying. In order to be consistent we expand the frequency-dependent susceptibility $\chi(\omega_l)$ in a Taylor series up to second order in the carrier frequency ω:

$$\chi(\omega_l)\cong\chi(\omega)+(\omega_l-\omega)\frac{\partial\chi}{\partial\omega}+\frac{(\omega_l-\omega)^2}{2}\frac{\partial^2\chi}{\partial\omega^2} , \tag{A3}$$

where χ is a slowly varying function of ω. Substituting (A3) into (A2) and recognizing that each power of $(\omega_l-\omega)$ in the summation is equivalent to $i\partial/\partial t$ of the summation, we obtain the following expression for p in the time domain:

$$p\cong\chi\mathscr{E}+i\frac{\partial\chi}{\partial\omega}\frac{\partial\mathscr{E}}{\partial t}-\frac{1}{2}\frac{\partial^2\chi}{\partial\omega^2}\frac{\partial^2\mathscr{E}}{\partial t^2} , \tag{A4}$$

where χ, $\partial\chi/\partial\omega$, and $\partial^2\chi/\partial\omega^2$ are all evaluated at the carrier frequency. Substituting (A1), (A2), and (A4) into the second-order Maxwell equation (2.10) and combining terms we obtain

$$\frac{\partial\mathscr{E}}{\partial z}+\frac{1}{v^g}\frac{\partial\mathscr{E}}{\partial t}+\left[\frac{1}{2ik}\right]\left\{\frac{\partial^2\mathscr{E}}{\partial z^2}-\left[\left[\frac{1}{v^g}\right]^2+k\frac{\partial}{\partial\omega}\left[\frac{1}{v^g}\right]\right]\frac{\partial^2\mathscr{E}}{\partial t^2}\right\}=0 , \tag{A5}$$

where we have used the definitions

$$\frac{1}{v^g}\equiv\frac{\partial k}{\partial\omega} , \tag{A6a}$$

$$k\equiv\frac{\eta\omega}{c} , \tag{A6b}$$

$$\eta^2\equiv 1+4\pi\chi , \tag{A6c}$$

and have accounted for the frequency dependence of the index of refraction, η. In (A5) we neglect terms proportional to $1/k$ in order to be consistent with the SVEPA. Therefore, the differential operator to lowest order is

$$\frac{\partial\mathscr{E}}{\partial z}+\frac{1}{v^g}\frac{\partial\mathscr{E}}{\partial t}+\frac{i}{2}\left[\frac{\partial}{\partial\omega}\left[\frac{1}{v^g}\right]\right]\frac{\partial^2\mathscr{E}}{\partial t^2}=0 , \tag{A7}$$

where the zero on the right side of (A7) for the Raman medium under consideration is really the nonlinear four-wave-mixing part of the polarization described in Sec. II B. For the problems studied in the text the second derivative term in (A7) is negligible. All terms in (A7) are consistent with Refs. 6 and 12–15.

*Present address: Los Alamos National Laboratory (Box 1663, Mail Stop J569), University of California, Los Alamos, New Mexico 87545.

[1]K. Drühl, R. G. Wenzel, and J. L. Carlsten, Phys. Rev. Lett. **51**, 1171 (1983); J. L. Carlsten, R. G. Wenzel, and K. Drühl, SPIE **380**, 201 (1983).

[2]F. Y. F. Chu and A. C. Scott, Phys. Rev. A **12**, 2060 (1975).

[3]N. Tan-no, T. Shirahata, K. Yokoto, and Inaba, Phys. Rev. A **12**, 159 (1975); T. M. Makhviladze, M. E. Sarychev, and L. A. Shelepin, Zh. Eksp. Teor. Fiz. **69**, 499 (1975) [Sov. Phys.—JETP **42**, 255 (1976)].

[4]D. J. Kaup, Physica **6D**, 143 (1983); H. Steudel, *ibid.* **6D**, 155 (1983); R. Meinel, Opt. Commun. **49**, 224 (1984).

[5]T. M. Makhviladze and M. E. Sarychev, Zh. Eksp. Teor. Fiz. **71**, 896 (1976) [Sov. Phys.—JETP **44**, 471 (1976)].

[6]A. Hasegawa, Appl. Opt. **23**, 3302 (1984), and references therein.

[7]J. L. Carlsten and R. G. Wenzel (private communication).

[8]R. G. Wenzel (private communication).

[9]L. Allen and J. H. Eberly, *Optical Resonance and Two-Level Atoms* (Wiley, New York, 1975).

[10]J. R. Ackerhalt, Phys. Rev. Lett. **46**, 922 (1981); SPIE **288**, 293 (1981).

[11]N. Bloembergen, *Nonlinear Optics* (Benjamin, Reading, Mass., 1965).

[12]V. E. Zakharov and A. B. Shabat, Zh. Eksp. Teor. Fiz. **61**, 118 (1971) [Sov. Phys.—JETP **34**, 62 (1972)].

[13]S. A. Akhmanov, A. S. Chirkin, K. N. Drabovich, A. I. Kovrigin, R. V. Khokhlov, and A. P. Sukhorukov, IEEE J. Quantum Electron. **QE-4**, 598 (1968).

[14]L. F. Mollenauer, R. H. Stolen, and J. P. Gordon, Phys. Rev. Lett. **45**, 1095 (1980).

[15]V. I. Karpman and E. M. Krushkal, Zh. Eksp. Teor. Fiz. **55**, 530 (1968) [Sov. Phys.—JETP **28**, 277 (1969)].